Spectroelectrochemical studies of TDMQ20: A potential drug against Alzheimer's disease

Magdalena Z. Wiloch [a,*], Martin Perez-Estebanez [b,*], Natalia Baran [a], Aranzazu Heras [b], Martin Jönsson-Niedziółka [a], Alvaro Colina [b]

[a] *Institute of Physical Chemistry, Polish Academy of Sciences, Kasprzaka 44/52, 01-224 Warsaw, Poland*
[b] *Department of Chemistry, University of Burgos, Pza. Misael Bañuelos s/n, E-09001 Burgos, Spain*

ARTICLE INFO

ABSTRACT

Alzheimer's Disease (AD), reported for the first time in 1906, is a common disease that remains incurable to this day. In the past, a family of treatments using Cu(II) chelators failed during clinical trials, evidencing the importance of pre-clinical studies. In this work, we performed electrochemical characterisation of TDMQ20, a new potential drug against AD, using electrochemistry and spectroelectrochemistry. On the basis of voltammetry, we determined that TDMQ20 undergoes a two-step irreversible oxidation process and a one-step irreversible reduction process. Both oxidation and reduction reactions are pH-sensitive. Bidimensional UV–Vis spectroelectrochemistry (UV–Vis-SEC) allowed us to confirm that oxidation of TDMQ20 can occur both on the aliphatic chain and on the aromatic ring. The results expand the knowledge of the TDMQ20 redox activity in the human body which is important from the point of view of the toxicity of the proposed therapy.

1. Introduction

Alzheimer's Disease (AD), first reported in 1906, nowadays is the most common cause of dementia amongst older people. According to the leading hypothesis, described in 1992 in Science and called the amyloid cascade hypothesis [1], overproduction of β-amyloid peptides (Aβ) are related to AD development. These peptides have three important features related to AD pathology: first of all, they aggregate very fast. For this reason, an abnormal increase of Aβ accumulation leads to their aggregation in the brain, forming oligomers and then amyloid plaques, which ultimately provokes neuronal dysfunction and the death of neurons. Secondly, they bind copper(II) ions, which accelerates the aggregation process. Finally, the Cu(II)-Aβ complexes catalyse the production of Reactive Oxygen Species (ROS) and Reactive Nitrogen Species (RNS) contributing to oxidative stress [2]. For the aforementioned reasons, there is great interest in the development of new therapeutic substances whose mechanism of action is based on two strategies: the removal of amyloid beta deposits from the brain or the extraction of Cu(II) ions. In 2021, the Aducanumab antibody directed against Aβ aggregates received its first approval in the USA for the treatment of AD [3]. Unfortunately, this drug is not suitable for all patients. Therefore, specific copper chelators are investigated as a good alternative. Up to now,

chelators such as clioquinol (CQ) and PBT2 have failed in clinical trials due to the formation of redox-active ternary complexes with Cu(II)-Aβ [4,5].

Presently, a new promising prototype ligand series, named TDMQ (tetradendate monoquinolines), is being studied intensively [6–14]. TDMQ ligands have an 8-aminoquinoline motif with a bidentate amine side chain attached to the quinoline moiety. This molecule structure provides the square planar tetradentate coordination sphere preferred for effective chelation and selectivity for copper(II) ions [9]. TDMQ molecules efficiently extract Cu(II) from Cu(II)-Aβ(1–42) complexes, creating new 1:1 metal:ligand complexes Cu(II)-TDMQ. Of all TDMQ ligands, TDMQ20 (Scheme 1) exhibits the highest affinity constant with Cu(II) ions [8]. The use of TDMQ20 exhibits many advantages: for example, it does not disturb the activity of metalloenzymes such as Cu-Zn-SOD, tyrosinase or metal-containing cofactors like vitamin B12 [10]. Also, the biomimetic oxidation of TDMQ20 leads to products fully soluble under aqueous experimental conditions which, therefore, probably do not accumulate in human body tissues [14]. The results of preclinical studies carried out in mice also showed the highest effectiveness of TDMQ20 in reducing oxidative stress [6]. For all these reasons, TDMQ20 could be considered as a good drug candidate for AD treatment.

However, to fully understand the possible reactions that TDMQ20
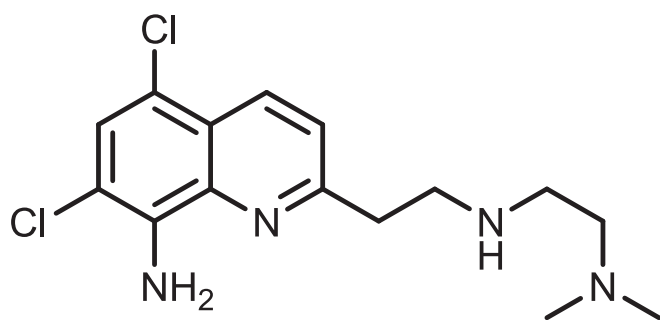
TDMQ20

Scheme 1. Structure of TDMQ20 molecule.

may undergo in the human body, the reactivity of this drug should be further characterised. Although some works can be found studying the chemical reactivity of TDQM20 [14], we found a lack of electrochemical studies conducted for TDMQ20. Electrochemistry allows for a fine control of the potential, which can help to fully characterise the reactivity of various substances towards redox changes. However, the information provided by electrochemistry can be greatly expanded by the addition of a spectroscopic technique that interrogates the processes taking place at the electrode. This strategy, named spectroelectrochemistry (SEC), is a truly powerful tool for the characterisation of complex systems [15]. Such studies would help to better understand what redox reactions the TDMQ20 molecule may undergo in the human body.

In this work, we performed comprehensive research combining voltammetric and UV–Vis absorption spectroelectrochemical techniques. Using voltammetry, we characterised the oxidation and reduction processes of TDMQ20 in detail and investigated the influence of pH on the redox reactivity of the tested molecules. Moreover, we have performed bidimensional thin-layer UV–Vis spectroelectrochemical experiments (Bidim-SEC). In a single Bidim-SEC experiment, two optical arrangements, normal and parallel, were used. The normal configuration, in which the light beam strikes perpendicular to the electrode surface [16,17], allows us to obtain information about both the diffusion layer and possible adsorption processes of TDMQ20 on the electrode surface. Parallel configuration, in which the light beam passes parallel to the electrode surface [18,19], provides information about changes to the tested compounds only in a small confined space adjacent to the working electrode surface.

2. Experimental section

2.1. Chemicals and materials

Inorganic compounds: disodium phosphate (Na_2HPO_4, 99,99 %), monosodium phosphate (NaH_2PO_4, 99,99 %), sodium hydroxide (NaOH, 99,9%), copper chloride ($CuCl_2$, 99,99 %) and hexaammineruthenium(III) chloride ($[Ru(NH_3)_6]Cl_3$, 98 %) were purchased from Merck and were used without further purification. All solutions used in (spectro)electrochemical and spectroscopic measurements were prepared with deionised water (resistivity of 18.2 MΩ·cm at 25 °C) from a NuZar U24 (RephiLe) purification system (experiments performed in Poland) and Milli-Q purification system (experiments performed in Spain). The TDMQ20 (N1-(2-(8-amino-5,7-dichloroquinolin-2-yl)ethyl)–N2,N2-dimethylethane-1,2-diamine hydrochloride) was purchased from Prochimia Surfaces.

2.2. Electrochemical methods

Electrochemical experiments on glassy carbon disk electrodes (Ø 3 mm, Mineral) were performed using an Autolab PGSTAT204 potentiostat (Metrohm AG) controlled by the NOVA software (version 2.1.5). CV measurements were performed at different scan rates and at least 3 scans were recorded for each series. The following parameters were used for SWV: step 2 mV, modulation amplitude 50 mV and frequency 25 Hz. Parameters for DPV measurements were as follows: step: 0.005 V, modulation amplitude 0.05 V, modulation time 0.1 s, and interval time 1 s. The acquisition of voltammetric curves was repeated at least 3 times for each solution of and TDMQ20. All experiments were performed in a three-electrode arrangement, with a Ag/AgCl (3 M NaCl) reference electrode, a platinum rod as the counter electrode, and a glassy carbon disk electrode (GCE) as the working electrode. The reference electrode was separated from the working solution by a salt bridge filled with a 0.1 M phosphate buffer solution with the same pH as in the cell. The potential of the reference electrode was calibrated based on the ruthenium electrode process. The formal potential of hexaammineruthenium (III/II) chloride in 0.5 M KNO_3 is 0.172 ± 0.002 V vs. Ag|AgCl|3 M NaCl. Prior to each voltammetric measurement the GCE was polished on a Buehler polishing cloth to a mirror-like surface, using aqueous slurries of 0.05 μm alumina powder followed by 1 min water ultrasonication to remove the remaining powder. All electrochemical measurements were carried out in 0.1 M phosphate buffer solution in the range of pH values from 3 to 8 every half pH unit. The pH was adjusted by pH-metric titration with small volumes of concentrated NaOH or H_3PO_4 solutions. The pH was closely monitored before and at the end of each voltammetric measurement. The solution was saturated with argon during the experiments at 25°C.

2.3. Spectroelectrochemical methods (SEC)

Thin-layer Bidim-SEC experiments were performed in custom-made cell designed for screen-printed electrodes (SPEs) described and tested previously [20]. In order to perform studies in parallel configuration, two bare optical fibres (100 μm in diameter, Ocean Optics) were attached to a quartz plate using nail polish. The first optical fibre was connected to the light source, and the second fibre was connected to the spectrophotometer to collect the light transmitted through the sample. The distance between the two fibres was $\ell = 1.6$ mm. The quartz plate was then placed on the SPE, creating a 0.21 μm thin-layer cell and ensuring that the optical fibres are placed adjacent and parallel to the working electrode. This configuration ensures a $w = 0.42$ mm normal optical path length. For normal configuration measurements, a reflection probe (RPROBE-VIS-UV, Metrohm-DropSens) was connected to the setup. An integration time of 1000 ms was used in the optical experiments. All experiments were performed at room temperature (in the presence of oxygen) using commercial carbon Screen-Printed Electrodes (C-SPEs) (DRP-110, MetrohmDropSens). Each C-SPE has a 4-mm diameter carbon working electrode (WE), a carbon counter electrode (CE) and a silver pseudo-reference electrode (RE).

Bidim-SEC experiments were carried out using two customised SPELEC instruments (Metrohm-DropSens). Each customised SPELEC equipment contains a halogen-deuterium lamp, a potentiostat and a suitable spectrophotometer. All of the components of the equipment are synchronised to ensure the correlation of electrochemical and spectroscopic techniques, ensuring reliable *operando* and time-resolved data acquisition. Both SPELEC devices were connected to each other to ensure the synchronisation of normal and parallel measurements. All measurements were performed using the DropView software (MetrohmDropSens).

2.4. UV–Vis spectroscopy

UV–Vis spectra were recorded at 25 °C on an Evolution 300

spectrophotometer (Thermo Scientific) over the spectral range of 210–900 nm. Quartz cuvettes with an optical path of 1 cm were used (Starna Scientific). TDMQ20 concentration was determined by UV–Vis titration using CuCl$_2$. Additionally, UV–Vis spectroscopy was used in order to characterise TDMQ20 deprotonation in phosphate buffer solutions. Samples containing TDMQ20 were titrated with NaOH in the pH range 3–8 by manual additions of the concentrated base solution.

3. Results and Discussion

3.1. Voltammetry of TDMQ20

According to recent reports, the TDMQ20 molecule can be readily oxidised to water-soluble metabolites, and therefore, this drug candidate might be easily metabolised and excreted in vivo. The catalytic oxidation of TDMQ20 was performed using a biomimetic system [14]. To better understand the oxidation of TDMQ20 we recorded the electrochemical response over a wide anodic range (from + 0.2 V up to + 1.5 V, Fig. 1). The experiments were performed in a phosphate buffer of pH 7.4 to reflect conditions in the human body. In the voltammogram, two consecutive oxidation processes, both irreversible, were observed: a well-defined peak at + 0.71 V and a broad and ill-defined oxidative wave over the + 0.8 – +1.1 V range (Fig. 1). Scanning at a faster scan rate did not improve the reversibility of these redox processes, which was diffusion-controlled (linear dependence of the peak current with the square root of scan rate, SI Figure S2.8.).

In order to test if the protonation of the molecule affects the oxidation process, we conducted tests over a wide range of pH from 3.0 up to 8.0 (Fig. 2 and SI Figure S 2.1). For the first oxidation, a peak shift to less positive potential was detected as the pH of the solution increased. The same phenomenon was observed for various quinolines [21–24]. The E_{pox} versus pH plot based on DPV (SI Fig. S2.3A), shows a linear dependence with the slope of 39 mV per pH unit, suggesting that the oxidation of TDMQ20 at GCE involves 2 electrons and 1 proton. Similarly to the first peak, the second signal was also influenced by the change in pH. However, this was not a linear relationship, and the shape of the obtained curves differed significantly from each other (Fig. 2), which suggests that the TDMQ20 oxidation process at different pH may lead to various oxidation products. Based on the oxidation potentials of TDMQ20, it can be speculated that this drug candidate is stable in the brain (where strong oxidants are not present). However, it can be oxidised in the liver through cytochrome P450 [14,25].
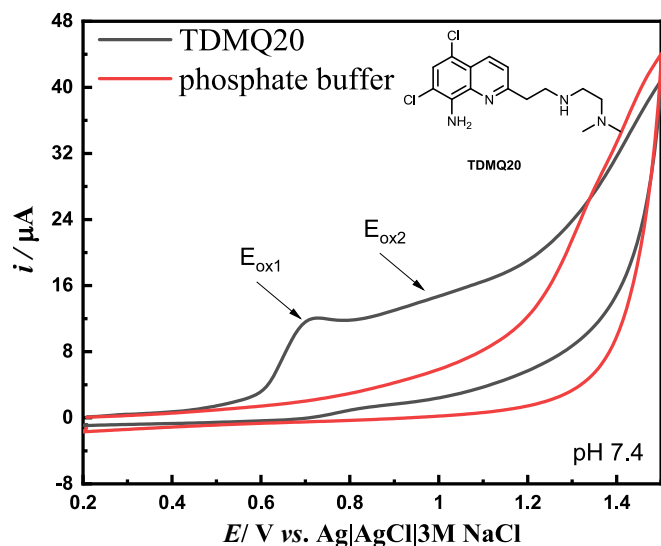
In order to test whether the first anodic process can be reversible, we have registered cyclic curves in a shorter potential range (from + 0.2 V up to + 1 V) at all pH values (Fig. 3). When CV was registered in the shorter potential window only one irreversible oxidation peak (except for pH 5.0 and 6.0) was detected. Scanning at a faster scan rate, as previously, did not improve the reversibility of the redox processes. SWV measurements also indicate that this process is not electrochemically reversible. In SWV the current is sampled in both positive and negative potential pulses, allowing us to obtain information from both oxidation and reduction processes almost simultaneously. When we plotted the forward and backward components of the total current (Figure SI 2.1A) we observed that the forward component of the current showed the peak at the same potential as the total current, while on the backward component, no cathodic peak occurred, which confirmed the irreversibility of first oxidation process on CV. The CV recorded for the solution at pH 5.0 and 6.0 (v = 100 mV/s) showed two oxidation peaks (Fig. 3). The same behaviour was observed in Fig. 2. At the beginning, we assumed that it could be related to the pKa of the tested molecule. However, TDMQ20 has two pKa values pK$_{a1}$ = 1.0 and pK$_{a2}$ = 8.0 [26]. Therefore, the two peaks are not related to the protonation change of TDMQ20. The splitting of peaks was observed for azo dye compounds derived from hydroxyquinolinone, and the authors of that study suggest the accompaniment of some adsorption component [27]. Interestingly, on DPV and CV at lower scan rates (v = 10 mV/s, pH 6.0 and 5.0, see SI Figure S2.6.), only one signal is observed. This suggests that the electron transfer process is quite fast and a higher scan rate was needed to observe the double peak [28].

In order to investigate the cathodic electrochemical behaviour of TDMQ20, the potential range of the CVs was extended to negative potentials. Cyclic voltammograms were recorded from + 0.2 V to −0.8, and up to + 0.9 V (Fig. 4A) or, in the reverse direction, from + 0.2 V to + 0.9 V and then a sweep to a negative potential of −0.8 V (Fig. 4B). When the measurement started at + 0.2 V and moved toward negative potentials, a reduction peak with very low current intensity was observed (Fig. 4A). An increase in the pH value of the supporting electrolyte caused a shift of the reduction peak towards more negative potential values (Figure S2.3). The same phenomenon was observed when DPV curves were recorded (see SI Fig. 2.1B). Even if reduction currents were much lower than that of the oxidation, the E_{red} versus pH plot based on DPV exhibits a slope of 36 mV per decade (SI Fig. S2.3A), which suggests that also here 2 electrons and one proton are involved in the process.

When the direction of the potential sweep was reversed (i.e. the sweeps goes from + 0.2 V towards more positive potentials), the same electrochemical response was obtained in the anodic range as described in Fig. 3. However, the electrochemical response below + 0.4 V was completely different (compared to Fig. 3A). As a result of the TDMQ20 oxidation, a new product was formed, which undergoes a two-step redox reaction. Therefore, two reduction ($E_{red'}$ = +0.02 V and $E_{red''}$ = − 0.1 V) and two oxidation ($E_{ox'}$ = +0.20 V and $E_{ox''}$ = + 0.09 V) peaks were present in the CVs (Fig. 4B). The differences between the anodic and the cathodic peaks potentials, $|E_{ox'} - E_{red'}| = 180$ mV and $|E_{ox''} - E_{red'}| = 190$ mV suggest that both processes exhibited slow kinetics. A similar behavior was observed for phenol by Enache and Oliviera-Brett [29] and Stević et al. for 8-hydroxyquinoline [21]. At the same time, as these peaks appear, the main oxidation peak current decreases with subsequent cycles due to the adsorption of TDMQ20 oxidation products on the GCE surface. Based on these measurements and the reports in the literature [21,29], we can conclude that the oxidation of TDMQ20 results in the formation of a redox-active chemisorbed species whose redox potential is lower than that of the TDMD20 molecule itself. In order to confirm our thesis, we performed a study using bidimensional thin-layer UV–Vis SEC, which will be described in the next section.

3.2. Bidimensional spectroelectrochemical behaviour of TDMQ20

To obtain more information about the processes taking place during

Fig. 1. CV (first scan) for **TDMQ20** recorded in 0.1 M phosphate buffer pH 7.4, **v = 0.1 V/s.**
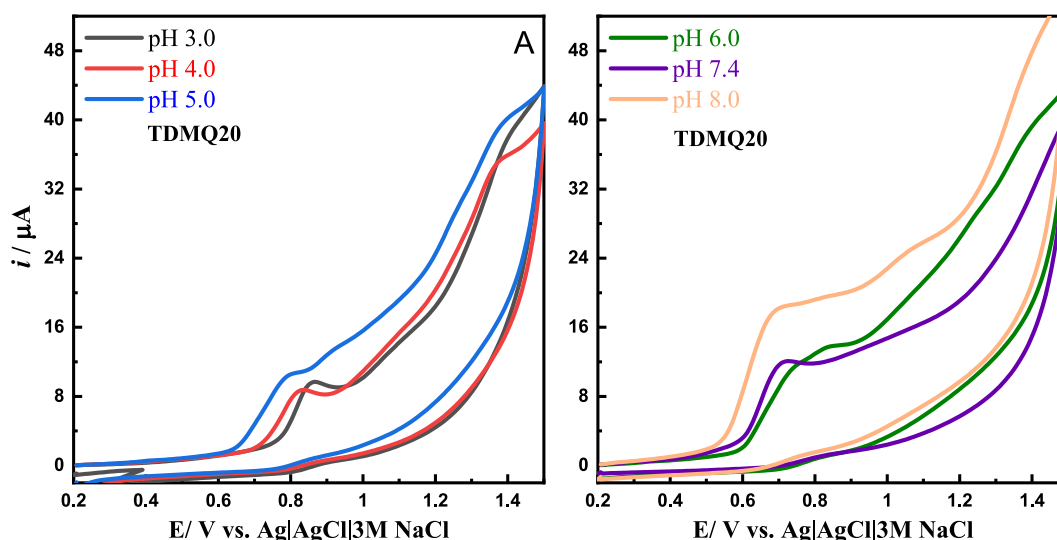
Fig. 2. CV (first scan) for **TDMQ20** (wider range of potentials) at pH (A) 3 to 5 and (B) 6 to 8, recorded in 0.1 M phosphate buffer, **v = 0.1 V/s.**
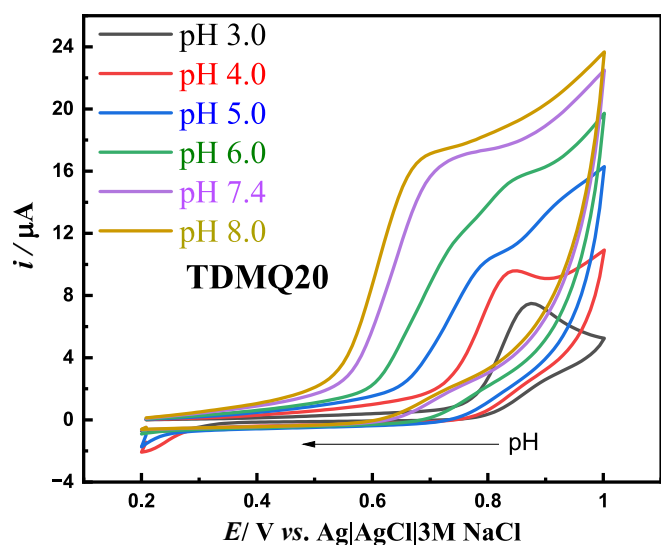
Fig. 3. CV (first scan) for (A) **TDMQ20** (narrow range of potentials) at pH range values 3.0 – 8.0 recorded in 0.1 M phosphate buffer, **v = 0.1 V/s.**

TDMQ20 oxidation, a study using bidimensional spectroelectrochemistry (Bidim-SEC) was carried out [30,31]. In this experiment, UV–Vis spectroelectrochemistry (UV–Vis-SEC) is used to obtain *operando* information about the processes taking place on the working electrode and the diffusion layer. More specifically, Bidim-SEC uses two complementary configurations to study the processes taking place in the system: parallel and normal. In the parallel configuration, a light beam is focused parallel to the WE using bare optical fibres to interrogate the solution adjacent to the electrode. Meanwhile, for the normal configuration, a reflection probe is used to focus a light beam on the surface in a near-normal mode, obtaining simultaneous information about the surface electrode and the diffusion layer [15]. A schematic of the used experimental setup is represented in Fig. 5A. The reason why we decided to use thin-layer is because it is the best way to limit the optical paths for both optical configurations in Bidim-SEC. In this way, we can define a closed system, allowing the correction of the optical signals, which is necessary in order to deconvolve the electrode process [32]. The presence of a semi-infinite diffusion layer could generate heterogeneous concentration profiles larger than the size of the optical fibers used in parallel configuration, making difficult the comparison of the information provided by the two configurations.

A CV was performed to study the oxidation of TDMQ20 with Bidim-SEC. The results are shown in Fig. 5B-D. Fig. 5B and C represent the contour plot of all the UV–Vis spectra registered during the experiment in normal and parallel configurations. For clarity, the CV is also represented in Fig. 5D. The CV obtained using C-SPE as electrode is slightly different to the one acquired using GCE. In this case, the second peak of oxidation, which was called E_{ox2} in Fig. 1, is better defined in the CV performed on C-SPE (Fig. 5D) which is most likely related to the slightly different surface structure of GC and C-SPE. Usually, the electron transfer is sluggish on C-SPEs respect to a GC electrode. During the backward scan, the reversible reduction of absorbed species is observed, as discussed in Fig. 4B.

As can be seen in Fig. 5B and C, during the oxidation of TDMQ20, noticeable changes in the parallel and normal UV–Vis spectra are registered. At 261 nm, corresponding with the absorbance maximum of TDMQ20 (Figure S1), a noticeable negative band is observed, which decreases during TDMQ20 oxidation. The presence of a negative band in UV–Vis-SEC indicates that a reactant has been consumed in the electrochemical process, since the reference spectrum is defined at the beginning of the experiment, being the solution containing TDMQ20 (therefore, changes of absorbance are measured). This band is observed in normal and parallel configuration, indicating that the TDMQ20 present in the solution is disappearing during its oxidation, as expected. Some variations of the absorbance at this wavelength can be observed at negative potentials, which will be discussed later.

In Fig. 5D (solid blue line) the evolution of the absorbance at this wavelenght during the CV is plotted. This kind of representation is known as VoltaAbsorptogram (VA). The VA at 261 nm in parallel configuration (VAp_{261}) confirms that the vanishing of the TDMQ20 takes places at potentials > +0.40 V. During the experiment, the evolution of other positive absorption bands, corresponding with the oxidation products of TDMQ20, is also observed (Fig. 5B and C). Two main absorption bands centered at 240 and 289 nm can be detected. The VAp_{289} reveals the evolution of this band during the oxidation of TDMQ20. Since this band is observed both in parallel and normal configuration, it can be concluded that this band corresponds to a soluble product of the oxidation of TDMQ20. Similar conclusions can be obtained for the band centered at 240 nm (VAp_{240}, Fig. 5D).

During the backward scan, at potentials <+0.2 V, two reversible processes of reduction are observed, as was discussed in Fig. 4B. Analysing the response of Bidim-SEC in parallel configuration (Fig. 5 D), it is observed that the absorbance at the three selected wavelengths (240,
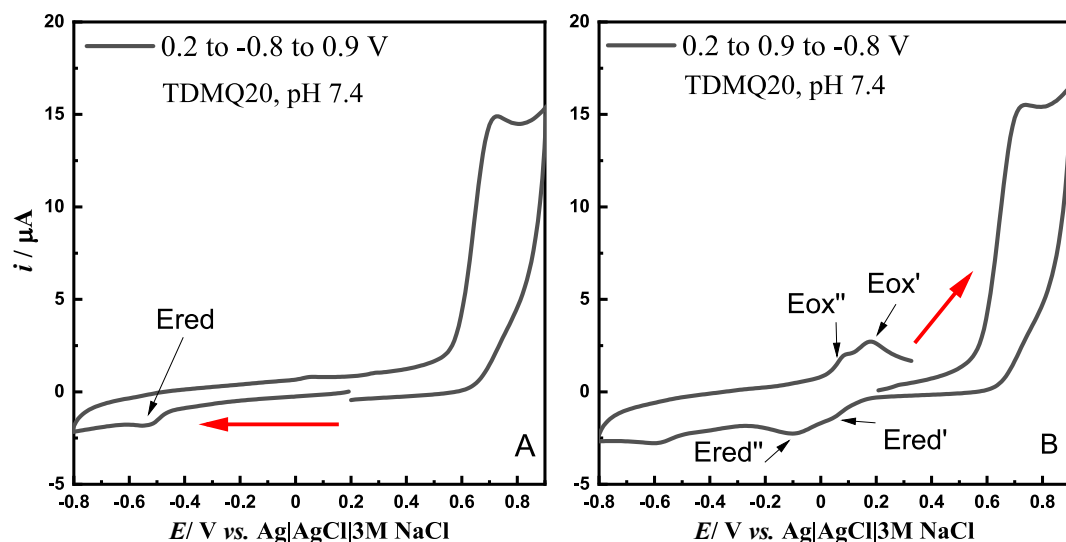
Fig. 4. CV for **TDMQ20** at pH 7.4 in two directions (A) 0.2 to −0.8 V up to 0.9 V and (B) from 0.2 to 0.9 up to −0.8 V recorded in 0.1 M phosphate buffer, **v = 0.1 V/s.**
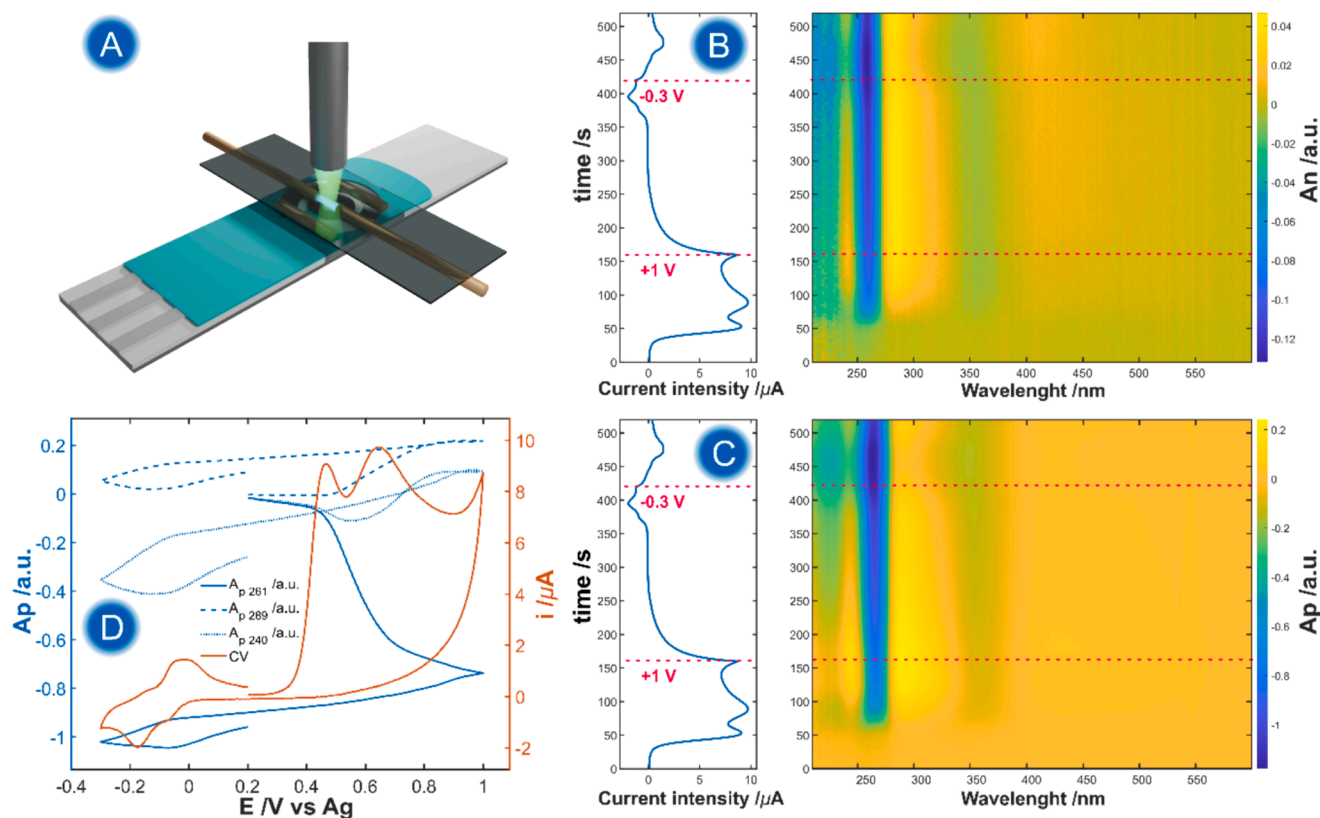
Fig. 5. (A) schematic of the experimental setup used for Bidim-SEC experiments in thin-layer configuration. (B, C) CV and contour plots of the registered spectra during the experiment in (B) normal and (C) parallel configuration. (D) CV and VA at different wavelengths in parallel configuration. Experimental conditions were: 0.5 mM TDMQ20 + 0.1 M phosphate buffer pH 7.4, **v = 0.005 V/s.** Experiment performed using C-SPE.

261, 289 nm) decreases reversibly during the reversible reduction observed at −0.20 V. This fact confirms that several oxidation products are being reduced in this process, as will be explained later.

By comparing the evolution of the spectra registered in normal and parallel configurations (Fig. 5 B and C), we find no noticeable differences between the spectra. This is counter-intuitive since electrochemistry demonstrates that during TDMQ20 oxidation, a modification of the electrode surface is observed (Fig. 4). In an ideal system, adsorption

processes on the WE should lead to changes in the absorbance in normal configuration during UV–Vis-SEC experiments. The explanation of this apparent paradox is that TDMQ20 can undergo different chemical changes during its oxidation, and many of them do not lead to changes in the UV–Vis spectra. This was proven by Nguyen et al.[14] who demonstrated that oxidation of the aliphatic chain of TDMQ20 does not significantly modify the UV–Vis spectrum of the molecule. Only modifications involving the quinolone ring were reported to influence the

absorbance spectra. Thus, it is possible that an electrochemical oxidation of TDMQ20 is taking place during the first steps of oxidation (+0.45 V, Fig. 5A), affecting the aliphatic chain of TDMQ20 (Scheme 1), adsorbing the molecule to the carbon WE surface, without affecting its UV–Vis spectra. This hypothesis can be confirmed by Bidim-SEC, comparing the information provided by normal and parallel configuration. By correcting the absorbance in normal configuration, An, with the absorbance in parallel configuration, Ap, (describe in details in SI) using the optical path-lengths as follows:

$$A_n^C = A_n - \frac{Ap \times w}{\ell} \tag{1}$$

The corrected absorbance in normal configuration at a given wavelength A_n^C, provides information about the processes taking place on the electrode surface, with minimal contribution from processes taking place in the solution [33]. Therefore, when studying the absorbance of a species formed in solution, the value of A_n^C should be close to zero. If the value of A_n^C changes significantly during the experiment, this variation must be related to processes taking place on the WE surface, since only the normal configuration interrogates the electrode surface [30].

In the experiment shown in Fig. 5, A_n^C at 289 nm remains close to 0 during all experiment, confirming that this absorption band corresponds to a soluble oxidation product formed during oxidation of TDMQ20 (Fig. 6, blue dotted line). While for 261 nm, the band corresponding to TDMQ20, a distinctly different behavior is observed, Fig. 6. When the absorbance is corrected (Fig. 6, blue solid line), a clear evolution of the voltabsorptogram corresponding to the corrected absorbance, VA_n^C, at 261 nm is observed, which is related to the electrochemical oxidation. This indicates that parallel configuration registers the conversion of the TDMQ20 to a soluble oxidation product which absorbs at different wavelength than TDMQ20, while in normal configuration not only this soluble product is observed, but also the generation of an insoluble product which absorbs at the same wavelength as the TDMQ20. This result agrees with our hypothesis, meaning that during oxidation of TDMQ20, part of the oxidised product is chemisorbed on the WE, probably by covalent interaction between the electrode and the N-containing groups of the aliphatic chain of TDMQ20.

In the potential range of + 0.2 to –0.3 V the VA_n^C at 261 nm exhibits some reversible changes related to the redox peaks centred at −0.10 V. These changes were already discussed for parallel configuration (Fig. 5D), concluding that this redox process involves some species present in solution. However, the corrected absorbance in normal configuration (VA_n^C) only provides information about processes taking place on the surface of the WE, suggesting that these voltametric peaks also involve the participation of species chemisorbed on the electrode surface. This can also be confirmed by electrochemical measurements, as discussed in Figure S.2.5.

Combining all the observations extracted from Bidim-SEC experiments, it can be concluded that TDMQ20 oxidation is a complex process taking place in multiple steps. The irreversible oxidation of TDMQ20 leads to the formation of a variety of products. Part of the products are irreversibly adsorbed on the C-SPE surface. This interaction probably happens through interaction with the N groups of the aliphatic chain of TDMQ20. Simultaneously, at least two soluble products are formed during the oxidation, as can be confirmed by the evolution of two positive bands at 240 and 289 nm with slight differences on its behavior (Fig. 5D). According to the existing literature, we have proposed a reaction scheme pointing out the possible oxidation products formed during electrochemical oxidation of TDMQ20 (scheme S1.1SI).

These observations are consistent with the reactivity of TDMQ20 previously reported. Recently, M. Nguyen and colaborators reported an interesting work where the chemical oxidation of TDMQ20 was carried out in several conditions [14]. According to the autors in the absence of a proper catalyst, the N-oxidation of the tertiary amine was favoured, leading to no significant change of the UV–Vis spectra. When an organometallic catalyst was added to the system, a wide variety of oxidation products were generated, many of them involving the loss of the primary amine attached to the quinolone ring. The generation of these products lead to a significant change of the UV–Vis spectra, wich a remarkable loss of absorbance at 261 nm (maximum of absorption for free TDMQ20) and generating new absorption bands at 241 and 330 nm. All of these observations are in agreement with the spectroelectrochemical results obtained: the first step of electrochemical oxidation leads to the N-oxidation of tertiary amine of TDMQ20, and generated a chemisorbed oxidation product without change in the UV–Vis spectra and passivating the electrode surface. During the second oxidation step, the oxidation of the aniline ring takes place, which triggers a chain of chemical reactions that leads to the formation of a variety of soluble compounds. In the literature, at least 10 different oxidation products have been reported resulting from the oxidation of the quinolone ring [14].

The processes observed at negative potentials after TDMQ20 oxidations are also very complex, involving the participation of both chemisorbed species on the WE surface and the free TDMQ20 and oxidation products present in solution, as is demonstrated by the Bidim-SEC measurements. The definition of these electrochemical process is not optimal, probable because chemisorbed species generated during the oxidation could be partially blocking the electrode surface, as confirmed by electrochemical measurements, where is observed that subsequent oxidation cycles lead to the passivation of the electrode surface (Figure S2.7). For this reason, the height of the voltammetric peaks in the reduction process is considerable lower than in the oxidation process.

4. Conclusions

Electrochemical and spectroelectrochemical studies of the TDMQ20 redox properties have been carried out. Based on voltammetry, the oxidation and reduction potentials of TDMQ20 have been determined. TDMQ oxidation occurs in two consecutive steps, which are irreversible, while for reduction, only one peak was visible on CV and DPV curves. The results show that both these processes are pH-sensitive: the increase of pH shifts oxidation and reduction potentials toward lower values. Bidimensional spectroelectrochemistry studies were instrumental in unravelling the electrochemical oxidation mechanism of TDMQ20. This multiresponse technique has provided unequivocal information related
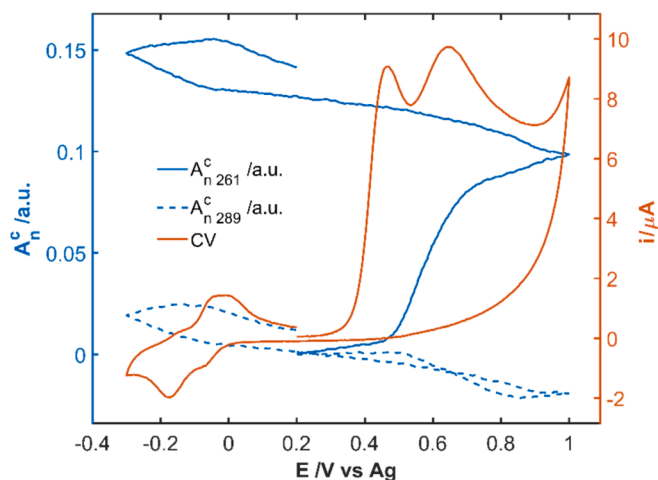
Fig. 6. CV and VA_n^C for 261 and 289 nm. Absorbance was corrected with the corresponding optical path-lengths. Experimental conditions were: 0.5 mM TDMQ20 + 0.1 M phosphate buffer pH 7.4, **v = 0.005 V/s**. Experiment performed using C-SPE.

to processes taking place on the electrode surface as well as in the solution adjacent to the electrode. Bidim-SEC shows that oxidation of TDMQ20 leads to the formation of a variety of products (N-oxide derivatives and dimeric quinone-imine derivatives). Combining voltammetry with spectroscopy, we showed that the first oxidation step is associated with the N-oxidation of the amines of the side chain, while the second step results from oxidation of the 8-aminoquinoline ring. The resented results are useful in understanding the redox conversion of TDMQ20, a potential drug candidate against AD, in the human body.

5. Data access

Data collected for this research is freely available in the repository RepOD.

CRediT authorship contribution statement

Magdalena Z. Wiloch: Writing – review & editing, Writing – original draft, Supervision, Methodology, Investigation, Funding acquisition, Formal analysis, Data curation, Conceptualization. **Martin Perez-Estebanez:** Writing – review & editing, Writing – original draft, Methodology, Investigation. **Natalia Baran:** Investigation. **Aranzazu Heras:** Writing – original draft. **Martin Jönsson-Niedziółka:** Writing – review & editing, Writing – original draft, Methodology, Investigation. **Alvaro Colina:** Writing – review & editing, Writing – original draft, Supervision, Conceptualization.

Declaration of competing interest

The authors declare that they have no known competing financial interests or personal relationships that could have appeared to influence the work reported in this paper.

Data availability

Data collected for this research is freely available in the repository RepOD.

Acknowledgements

Appendix A. Supplementary data

Supplementary data to this article can be found online at https://doi.org/10.1016/j.bioelechem.2024.108814.

References

[1] J.A. Hardy, G.A. Higgins, Alzheimer's disease: the amyloid cascade hypothesis, Science 256 (1992) 184–185, https://doi.org/10.1126/science.1566067.

[2] C. Cheignon, M. Tomas, D. Bonnefont-Rousselot, P. Faller, C. Hureau, F. Collin, Oxidative stress and the amyloid beta peptide in Alzheimer's disease, Redox Biol. 14 (2018) 450–464, https://doi.org/10.1016/j.redox.2017.10.014.

[3] S. Dhillon, Aducanumab: First Approval, Drugs 81 (2021) 1437–1443, https://doi.org/10.1007/s40265-021-01569-z.

[4] M. Mital, I.A. Zawisza, M.Z. Wiloch, U.E. Wawrzyniak, V. Kenche, W. Wróblewski, W. Bal, S.C. Drew, Copper Exchange and Redox Activity of a Prototypical 8-Hydroxyquinoline: Implications for Therapeutic Chelation, Inorg. Chem. 55 (2016) 7317–7319, https://doi.org/10.1021/acs.inorgchem.6b00832.

[5] S.C. Drew, Chelator PBT2 Forms a Ternary Cu2+ Complex with β-Amyloid That Has High Stability but Low Specificity, Int. J. Mol. Sci. 24 (2023) 9267, https://doi.org/10.3390/ijms24119267.

[6] J. Zhao, Q. Shi, H. Tian, Y. Li, Y. Liu, Z. Xu, A. Robert, Q. Liu, B. Meunier, TDMQ20, a Specific Copper Chelator, Reduces Memory Impairments in Alzheimer's Disease Mouse Models, ACS Chem. Nerosci. 12 (2021) 140–149, https://doi.org/10.1021/acschemneuro.0c00621.

[7] W. Zhang, Y. Liu, C. Hureau, A. Robert, B. Meunier, N4-Tetradentate Chelators Efficiently Regulate Copper Homeostasis and Prevent ROS Production Induced by Copper-Amyloid-β1–16, Chem. – Eur. J. 24 (2018) 7825–7829, https://doi.org/10.1002/chem.201801387.

[8] W. Zhang, D. Huang, M. Huang, J. Huang, D. Wang, X. Liu, M. Nguyen, L. Vendier, S. Mazères, A. Robert, Y. Liu, B. Meunier, Preparation of Tetradentate Copper Chelators as Potential Anti-Alzheimer Agents, ChemMedChem 13 (2018) 684–704, https://doi.org/10.1002/cmdc.201700734.

[9] W. Zhang, M. Huang, C. Bijani, Y. Liu, A. Robert, B. Meunier, Synthesis and characterisation of copper-specific tetradentate ligands as potential treatment for Alzheimer's disease, Comptes Rendus Chim. 21 (2018) 475–483, https://doi.org/10.1016/j.crci.2018.01.005.

[10] J. Huang, M. Nguyen, Y. Liu, A. Robert, B. Meunier, The TDMQ Regulators of Copper Homeostasis Do Not Disturb the Activities of Cu, Zn-SOD, Tyrosinase, or the Co^{II}I Cofactor Vitamin B12, Eur. J. Inorg. Chem. 2019 (2019) 1384–1388, https://doi.org/10.1002/ejic.201801332.

[11] M. Nguyen, A. Robert, A. Sournia-Saquet, L. Vendier, B. Meunier, Characterization of New Specific Copper Chelators as Potential Drugs for the Treatment of Alzheimer's Disease, Chem. – Eur. J. 20 (2014) 6771–6785, https://doi.org/10.1002/chem.201402143.

[12] M. Nguyen, L. Rechignat, A. Robert, B. Meunier, The Necessity of Having a Tetradentate Ligand to Extract Copper(II) Ions from Amyloids, ChemistryOpen 4 (2015) 27–31, https://doi.org/10.1002/open.201402075.

[13] M. Nguyen, C. Bijani, N. Martins, B. Meunier, A. Robert, Transfer of Copper from an Amyloid to a Natural Copper-Carrier Peptide with a Specific Mediating Ligand, Chem. – Eur. J. 21 (2015) 17085–17090, https://doi.org/10.1002/chem.201502824.

[14] M. Nguyen, Y. Li, A. Robert, Y. Liu, B. Meunier, Oxidation of TDMQ20, a Specific Copper Chelator as Potential Drug Against Alzheimer's Disease, ChemistrySelect 8 (2023) e202204877.

[15] J. Garoz-Ruiz, J.V. Perales-Rondon, A. Heras, A. Colina, Spectroelectrochemical Sensing: Current Trends and Challenges, Electroanalysis 31 (2019) 1254–1278, https://doi.org/10.1002/elan.201900075.

[16] I.S. Zavarine, C.P. Kubiak, A versatile variable temperature thin layer reflectance spectroelectrochemical cell, J. Electroanal. Chem. 495 (2001) 106–109, https://doi.org/10.1016/S0022-0728(00)00394-6.

[17] E. Muñoz, Á. Colina, A. Heras, V. Ruiz, S. Palmero, J. López-Palacios, Electropolymerization and characterisation of polyaniline films using a spectroelectrochemical flow cell, Anal. Chim. Acta 573–574 (2006) 20–25, https://doi.org/10.1016/j.aca.2006.01.029.

[18] A. Heras, A. Colina, V. Ruiz, J. López-Palacios, UV-Visible Spectroelectrochemical Detection of Side-Reactions in the Hexacyanoferrate(III)/(II) Electrode Process, Electroanalysis 15 (2003) 702–708, https://doi.org/10.1002/elan.200390088.

[19] H. Isago, A new spectroelectrochemical cell with a long optical path length for redox studies of phthalocyanines, J. Porphyr. Phthalocyanines 10 (2006) 1125–1131, https://doi.org/10.1142/s1088424606000478.

[20] J. Garoz-Ruiz, C. Guillen-Posteguillo, A. Heras, A. Colina, Simplifying the assessment of parameters of electron-transfer reactions by using easy-to-use thin-layer spectroelectrochemistry devices, Electrochem. Commun. 86 (2018) 12–16, https://doi.org/10.1016/j.elecom.2017.11.001.

[21] M.C. Stević, L.M. Ignjatović, G. Ćirić-Marjanović, S.M. Stanišić, M. Stanković, J. Zima, Voltammetric Behaviour and Determination of 8-Hydroxyquinoline Using a Glassy Carbon Paste Electrode and the Theoretical Study of its Electrochemical Oxidation Mechanism, Int. J. Electrochem. Sci. 6 (2011).

[22] Z.P. Yang, M. Alafandy, K. Boutakhrit, J.-M. Kauffmann, J. Arcos, Electrochemical oxidation of 8-hydroxyquinoline and selective determination of tin(II) at solid electrodes, Electroanalysis 8 (1996) 25–29, https://doi.org/10.1002/elan.1140080106.

[23] M.C. Stević, G. Ćirić-Marjanović, B. Marjanović, L.M. Ignjatović, D. Manojlović, The Electrochemical Oxidation of 6-Aminoquinoline: Computational and Voltammetric Study, J. Electrochem. Soc. 159 (2012) G151–G159, https://doi.org/10.1149/2.004212jes.

[24] A. Stoica, J. Zima, J. Barek, Differential Pulse Voltammetric Determination of 8-Aminoquinoline Using Carbon Paste Electrode, Anal. Lett. 38 (2005) 149–156, https://doi.org/10.1081/AL-200043471.

[25] P. Anzenbacher, E. Anzenbacherová, Cytochromes P450 and metabolism of xenobiotics, Cell. Mol. Life Sci. CMLS 58 (2001) 737–747, https://doi.org/10.1007/PL00000897.

[26] Y. Li, M. Nguyen, M. Baudoin, L. Vendier, Y. Liu, A. Robert, B. Meunier, Why Is Tetradentate Coordination Essential for Potential Copper Homeostasis Regulators in Alzheimer's Disease? Eur. J. Inorg. Chem. 2019 (2019) 4712–4718, https://doi.org/10.1002/ejic.201900951.

[27] A.S. Al-Gorair, R.N. Felaly, S.S. Al-Juaid, S.A. El Wanees, E.M. Mabrouk, M. Abdallah, Synthesis and voltammetric studies of azo dye compounds derived from 3-hydroxyquinolin-2-one in aqueous media, Int. J. Electrochem. Sci. 19 (2024) 100438, https://doi.org/10.1016/j.ijoes.2023.100438.

[28] V. Mirčeski, Charge Transfer Kinetics in Thin-Film Voltammetry. Theoretical Study under Conditions of Square-Wave Voltammetry, J. Phys. Chem. B 108 (2004) 13719–13725, https://doi.org/10.1021/jp0487152.

[29] T.A. Enache, A.M. Oliveira-Brett, Phenol and para-substituted phenols electrochemical oxidation pathways, J. Electroanal. Chem. 655 (2011) 9–16, https://doi.org/10.1016/j.jelechem.2011.02.022.

[30] D. Izquierdo, V. Ferraresi-Curotto, A. Heras, R. Pis-Diez, A.C. Gonzalez-Baro, A. Colina, Bidimensional Spectroelectrochemistry: application of a new device in the study of a o-vanillin-copper(II) complex, Electrochim. Acta 245 (2017) 79–87, https://doi.org/10.1016/j.electacta.2017.05.105.

[31] F. Olmo-Alonso, J. Garoz-Ruiz, A. Heras, A. Colina, Normal or parallel configuration in spectroelectrochemistry? Bidimensional spectroelectroanalysis in

presence of an antioxidant compound, J. Electroanal. Chem. 935 (2023) 117333, https://doi.org/10.1016/j.jelechem.2023.117333.

[32] F. Olmo, J. Garoz-Ruiz, A. Colina, A. Heras, Derivative UV/Vis spectroelectrochemistry in a thin-layer regime: deconvolution and simultaneous quantification of ascorbic acid, dopamine and uric acid, Anal. Bioanal. Chem. 412 (2020) 6329–6339, https://doi.org/10.1007/s00216-020-02564-1.

[33] J. López-Palacios, A. Colina, A. Heras, V. Ruiz, L. Fuente, Bidimensional spectroelectrochemistry, Anal. Chem. 73 (2001) 2883–2889, https://doi.org/10.1021/ac0014459.